







MvKeTR: Chest CT Report Generation with Multi-View Perception and Knowledge Enhancement

Xiwei Deng , Xianchun He , Yudan Zhou , Shuhui Cai , Congbo Cai , and Zhong Chen 

Abstract—CT report generation (CTRG) aims to automatically generate diagnostic reports for 3D volumes, relieving clinicians' workload and improving patient care. Despite clinical value, existing works fail to effectively incorporate diagnostic information from multiple anatomical views and lack related clinical expertise essential for accurate and reliable diagnosis. To resolve these limitations, we propose a novel Multi-view perception Knowledge-enhanced TansfoRmer (MvKeTR) to mimic the diagnostic workflow of clinicians. Just as radiologists first examine CT scans from multiple planes, a Multi-View Perception Aggregator (MVPA) with view-aware attention effectively synthesizes diagnostic information from multiple anatomical views. Then, inspired by how radiologists further refer to relevant clinical records to guide diagnostic decision-making, a Cross-Modal Knowledge Enhancer (CMKE) retrieves the most similar reports based on the query volume to incorporate domain knowledge into the diagnosis procedure. Furthermore, instead of traditional MLPs, we employ Kolmogorov-Arnold Networks (KANs) with learnable nonlinear activation functions as the fundamental building blocks of both modules to better capture intricate diagnostic patterns in CT interpretation. Extensive experiments on the public CTRG-Chest-548K dataset demonstrate that our method outpaces prior state-of-the-art models across all metrics.

Index Terms—Chest CT, Knowledge enhancement, Kolmogorov-Arnold networks, Radiology report generation, Multi-view learning.

I. INTRODUCTION

IN clinical practice, medical imaging plays an indispensable role, serving as a cornerstone for disease diagnosis, report writing, and subsequent decision-making. After acquiring a patient's radiology images, physicians examine all anatomical structures and regions of concern, then employ related expert knowledge to write a hand-crafted, clinically coherent report that documents the observations [1]. As evidenced in Fig. 1, such a radiology report typically comprises a findings section that describes thorough medical observations, followed by an

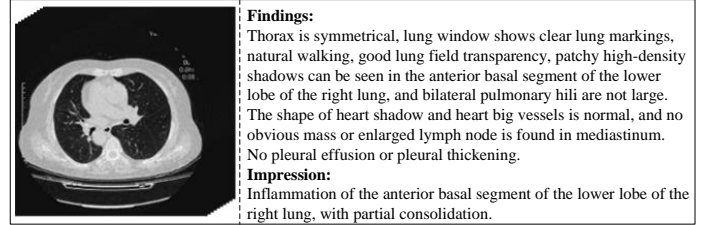


Fig. 1. An example of chest CT volume and its corresponding report, including findings and impression.

impression summarizing the most significant observations. The process of report writing is time-intensive and error-prone for clinicians [2]–[4]. Hence, the automation of report generation holds substantial value in lightening the burden of physicians and improving the quality of reports.

Despite recent advancements, there remain several constraints in previous studies that have not been fully addressed: (i) Ineffective incorporation of diagnostic information from multiple anatomical views. In comparison with 2D imaging [5], [6], 3D medical imaging (e.g., chest CT) provides a more holistic view of anatomical detail and spatial information, preserving the volumetric nature of the human body [7]. Furthermore, unlike a single view of 3D volumes [8]–[10], the multi-view nature of CT scans enables physicians to examine the patient's condition from different anatomical views - axial, sagittal, and coronal- allowing for a more accurate diagnosis of many diseases. As a common example, pulmonary nodules, especially smaller ones, may be easily obscured by adjacent structures or misdiagnosed when viewed from a single perspective [11]. Axial views might reveal the presence of a nodule, but coronal and sagittal views are crucial for accurately assessing its characteristics and relationships to surrounding tissues [12], thereby enhancing differential diagnosis [13]. (ii) Absence of pertinent medical knowledge crucial for precise and dependable diagnosis. Relying merely on radiology images for report writing may be sub-optimal, overlooking the critical medical expertise [9], [14]. Experienced clinicians usually consult analogous case reports to extricate insights into diagnostic patterns and imaging features, guiding their decision-making when faced with complex or ambiguous cases during the diagnostic process. This knowledge-driven approach is critical for interpreting imaging findings, identifying subtle abnormalities, and writing clinically accurate reports.

Motivated by the aforementioned observations, we develop a novel Multi-view perception Knowledge-enhanced Trans-

This work was supported by the National Natural Science Foundation of China (Grant No. 22161142024, 12375291, and 82071913). (Corresponding authors: Congbo Cai; Zhong Chen.)

Xiwei Deng, Xianchun He, and Yudan Zhou are with the Institute of Artificial Intelligence, Xiamen University, Xiamen 361005, China (e-mail: xiweideng@stu.xmu.edu.cn; hexianchun@stu.xmu.edu.cn; ydzhou@stu.xmu.edu.cn).

Shuhui Cai, Congbo Cai, and Zhong Chen are with the Department of Electronic Science, Xiamen University, Xiamen 361005, China (e-mail: shcai@xmu.edu.cn; cbcai@xmu.edu.cn; chenz@xmu.edu.cn).

former (MvKeTR) to overcome the deficiencies of current methods. In particular, to mirror how radiologists examine 3D CT volumes from multiple anatomical planes, we initially design a Multi-View Perception Aggregator (MVPA) that utilizes view-aware attention to synthesize diagnostic information from different anatomical views effectively. To bridge the medical knowledge gap, we introduce a Cross-Modal Knowledge Enhancer (CMKE) that retrieves the most similar historical reports, analogous to how physicians consult relevant clinical records. Additionally, we employ Kolmogorov-Arnold Networks (KANs) [15], which feature learnable nonlinear activation functions, to learn the complicated diagnostic relationships inherent in CT interpretation. Extensive experiments on the public CTRG-Chest-548K dataset showcase that our proposed MvKeTR surpasses previous state-of-the-art methods across all established metrics.

In general, the main contributions of our work can be summarized as follows:

- 1) We propose a novel Multi-view perception Knowledge-enhanced Transformer (MvKeTR) to achieve higher-quality CT report generation. To the best of our knowledge, MvKeTR is the first attempt to utilize multi-view diagnostic information, cross-modal medical expertise, and the potential of emerging KANs in this way.
- 2) We recognize the inability of multi-view comprehension of current works and design a Multi-View Perception Aggregator that aggregates diagnostic information from multiple anatomical views, capturing comprehensive spatial features effectively.
- 3) We introduce a Cross-Modal Knowledge Enhancer that leverages relevant reports to incorporate domain expertise into the report generation process, improving the clinical relevance and accuracy of the predicted reports.
- 4) Extensive comparison and ablation experiments showcase the superiority of our method over the recent state-of-the-art (SOTA) models.

The remainder of this paper is structured as follows. Section II reviews the related work. Section III describes our proposed model in detail. Section IV presents experimental results on a publicly available dataset. Section V concludes our work and points out crucial future work.

II. RELATED WORK

A. Image Captioning

Image captioning [16], [17] aims to describe an image with a brief sentence. In image captioning, researchers mainly used rule-based methods to create image descriptions. Early approaches to image captioning predominantly adopted the encoder-decoder architecture [18]–[20]. The emergence of Transformer [21] has substantially propelled progress in image captioning field. Xu et al. [22] created an attention-based model trained via a dual approach - deterministic back-propagation and stochastic maximization of a variational lower bound. Li et al. [23] proposed GLA that generates relevant sentences by fusing object-level local representations and image-level global representations. Lu et al. [24] employed an adaptive attention model with a visual sentinel, enabling dynamic

determination of whether and where to focus on the input images during sequential word generation. Cornia et al. [25] completely exploited multi-modal contexts and multi-level information using a meshed transformer with memory. Liu et al. [26] reframed image captioning as a sequence-to-sequence prediction problem and proposed a caption transformer model. This transformer takes serialized input images and instills global contextual awareness across encoder layers from the outset while entirely eschewing convolutions. The techniques mentioned above have predominantly been explored within the 2D image domain, with 3D image captioning methodologies remaining relatively sparse thus far.

B. Medical Report Generation

The generation task of radiology report can be regarded as the derivative task of image captioning. Due to the encoder-decoder architecture's notable success in image captioning, numerous studies have utilized this method to produce medical image reports [27]–[30]. For example, Xue et al. [31] proposed MRMA, which circularly combines CNN and LSTM and constantly uses old sentences to generate new and coherent reports. Because transformer can capture the global and long dependencies of the entire input sequence, many researchers use it to improve the CNN-RNN structures, improving the accuracy of report generation and processing efficiency. Nooralahzadeh et al. [32] introduced M2TR, which is a progressive (from image to text to text) generative architecture that first extracts global feature-level context representations, then utilizes a large language model to generate comprehensive reports. Chen et al. [5] designed R2GenCMN, which employs a shared memory matrix to capture the alignment between image and text, facilitating cross-modal interaction and generation through memory querying and retrieval. Yang et al. [33] developed M2KT, which leverages a learnable medical knowledge base and multi-modal alignment mechanism to comprehensively learn visual features, enabling automated generation of radiology reports. Yi et al. [34] implemented TSGET, which incorporates two global enhancement layers in the transformer. The first layer captures global visual context, while the second layer refines global and regional features to obtain more comprehensive visual information. Yi et al. [35] presented UDT, which obtains disease tag features via clustering and then fuses these with the attended visual features to assist report generation. Wang et al. [36] constructed CAMANet, which designed a class activation map guided attention network that explicitly facilitates alignment and enhances the acquisition of disease-pertinent feature representations by harnessing aggregate class activation maps. These methods are limited to 2D image domains and have not been extended to 3D applications, researchers are now shifting their focus towards 3D report generation. Tang et al. [8] introduced SL-DG, a dual-module framework for CT scan report generation, consisting of a self-attention-based scan localizer (SL) for salient lesion feature extraction and a dynamic generator (DG) for report recommendation and synthesis. Hamamci et al. [9] established CT2rep, a framework that generates 3D medical reports using a novel auto-regressive

TABLE I
KEY NOTATIONS

Notations	Descriptions
X	The input 3D CT volume.
N_p	The number of extracted CT patches.
N_r	The number of reports in the CT report bank.
$\Phi_{ve}^a, \Phi_{ve}^c, \Phi_{ve}^s$	The axial, coronal, and sagittal CT-ViT.
X^a, X^c, X^s	The axial, coronal, and sagittal 3D CT volume.
Z^a, Z^c, Z^s	The axial, coronal, and sagittal embedded CT tokens.
B	The batch size.
D	The dimension of the embedding.
h, w	The height and width of the CT slices
P_t	The temporal patch size.
P_h, P_w	The spatial patch sizes of height and width.
N_t	The number of temporal patches.
$Z_{\text{top-}k}$	The retrieved top- k report embeddings.
F_{ke}	The features encoded by cross-modal knowledge enhancer.
F_{mv}	The features encoded by multi-view perception aggregator.
γ	The model parameters.
Φ_k	Nonlinear learnable parameters of the k^{th} KAN Layer.
E_v	The view embedding of anatomical view v .

causal transformer. They also developed a variant capable of processing longitudinal multi-modal data, leveraging a cross-attention-based multi-modal fusion module and hierarchical memory. Chen et al. [10] introduced Dia-llama. This framework harnesses the LLaMA2-7B model, transforming images into diagnostic cues to guide the generation of CT reports. It further incorporates a disease-aware attention mechanism, enabling the model to modulate its focus in response to varying pathological conditions dynamically. Therefore, it is difficult for traditional image caption methods to generate lengthy radiological reports that aim to describe the image in a short sentence. Thus, the domain of radiology report generation still harbors considerable scope for advancement and innovation.

III. METHODOLOGY

In this section, we describe our proposed MvKeTR model in detail. Table I illustrates the key notations and their respective descriptions adopted in this study.

A. Overview of the Proposed Approach

The generation of radiology reports can be considered an image-to-text problem, for which we follow a sequence-to-sequence paradigm. In doing so, unlike previous approaches [8], [10] that typically process a single-view image, our network handles the input 3D CT volume $X \in \mathbb{R}^{(224) \times 224 \times 224}$ by transforming it into three source sequences of CT patches: $Z^v = \{z_1^v, z_2^v, \dots, z_{N_p}^v\}$, $z_n^v \in \mathbb{R}^{(8) \times 8 \times 8}$, where $v \in \{a, c, s\}$ represents the axial, coronal, and sagittal views respectively, Z^v are embedded CT tokens extracted by 3D visual extractor for each view, and D is the dimension of the embedding. We regard the corresponding report as the target sequence $Y = \{y_1, y_2, \dots, y_L\}$, where $y_l \in \mathbb{V}$ are the predicted tokens, L the length of predicted tokens and \mathbb{V} the vocabulary of all possible tokens. Thus, the aforementioned process of report generation can be formalized as follows:

$$\log p(Y|X) = \sum_{l=1}^T \log p(y_l | y_1, \dots, y_{l-1}, X) \quad (1)$$

Subsequently, the model is trained to maximize $p(Y|X)$ by the negative conditional log-likelihood of Y given X :

$$\gamma^* = \arg \max_{\gamma} \sum_{l=1}^T \log p(y_l | y_1, \dots, y_{l-1}, X; \gamma) \quad (2)$$

where γ is the parameters of the model. The overall architecture of our proposed framework is illustrated in Fig. 2, where the contributions of each component are detailed in the following subsections.

B. 3D Visual Extractor

Following the previous work [9], CT-ViT is employed to extract embedded CT tokens $Z^v \in \mathbb{R}^{8 \times 8 \times 8 \times 512}$, by initially extracting $(28) \times 28 \times 28$ non-overlapping patches from the given 3D CT volume X^v , where $v \in \{a, c, s\}$. Then, each patch is embedded in a D -dimensional space, reshaped, and linearly transformed to an intermediate tensor $T_i \in \mathbb{R}^{B \times N_t \times \frac{h}{P_h} \times \frac{w}{P_w} \times D}$. Here, P_t represents the temporal patch size, B the batch size, N_t the temporal patch count, h and w correspond to the height and width of the CT slices, and D the dimension of the embedding space. P_h and P_w denote the spatial patch sizes of height and width. Subsequently, T_i is processed and reshaped to the final outcome tensor $T_o \in \mathbb{R}^{(\frac{h}{P_h} \cdot \frac{w}{P_w}) \times (B \cdot N_t) \times D}$ consecutively by the spatial and causal transformer models. The 3D visual extractor is composed of three independent CT-ViTs, which process the axial, coronal, and sagittal view CT volume, respectively. Fig. 3 illustrates the pipeline of visual feature extraction through CT-ViT.

The whole procedure can be formally formulated as:

$$Z^a = \{z_1^a, z_2^a, \dots, z_{N_p}^a\} = \Phi_{ve}^a(X^a) \quad (3)$$

$$Z^c = \{z_1^c, z_2^c, \dots, z_{N_p}^c\} = \Phi_{ve}^c(X^c) \quad (4)$$

$$Z^s = \{z_1^s, z_2^s, \dots, z_{N_p}^s\} = \Phi_{ve}^s(X^s) \quad (5)$$

where N_p denotes the number of extracted CT patches, $\Phi_{ve}^a(\cdot)$, $\Phi_{ve}^c(\cdot)$, and $\Phi_{ve}^s(\cdot)$ denote the axial, coronal, and sagittal CT-ViT, respectively.

C. KAN as Nonlinear Learner

Multi-layer perceptrons (MLPs) [37], [38] serve as basic blocks of contemporary deep learning models and prevail in numerous tasks (e.g., radiology report generation). However, these models often struggle with learning intricate nonlinear patterns in high-dimensional data, particularly in biomedical applications [39], where complicated interactions between features are common.

Unlike traditional MLPs that employ fixed activation functions at their nodes, KANs introduce learnable activation functions at the edges [15]. This simple modification enables KANs to achieve similar or superior accuracy in function-fitting tasks, even with fewer parameters than larger MLPs. Given an input \mathbf{x} , a KAN network is a stack of multiple KAN layers (as illustrated in Fig. 4), which can be characterized as:

$$\text{KAN}(\mathbf{x}) = (\Phi_{k-1} \circ \Phi_{k-2} \circ \dots \circ \Phi_1 \circ \Phi_0) \mathbf{x} \quad (6)$$

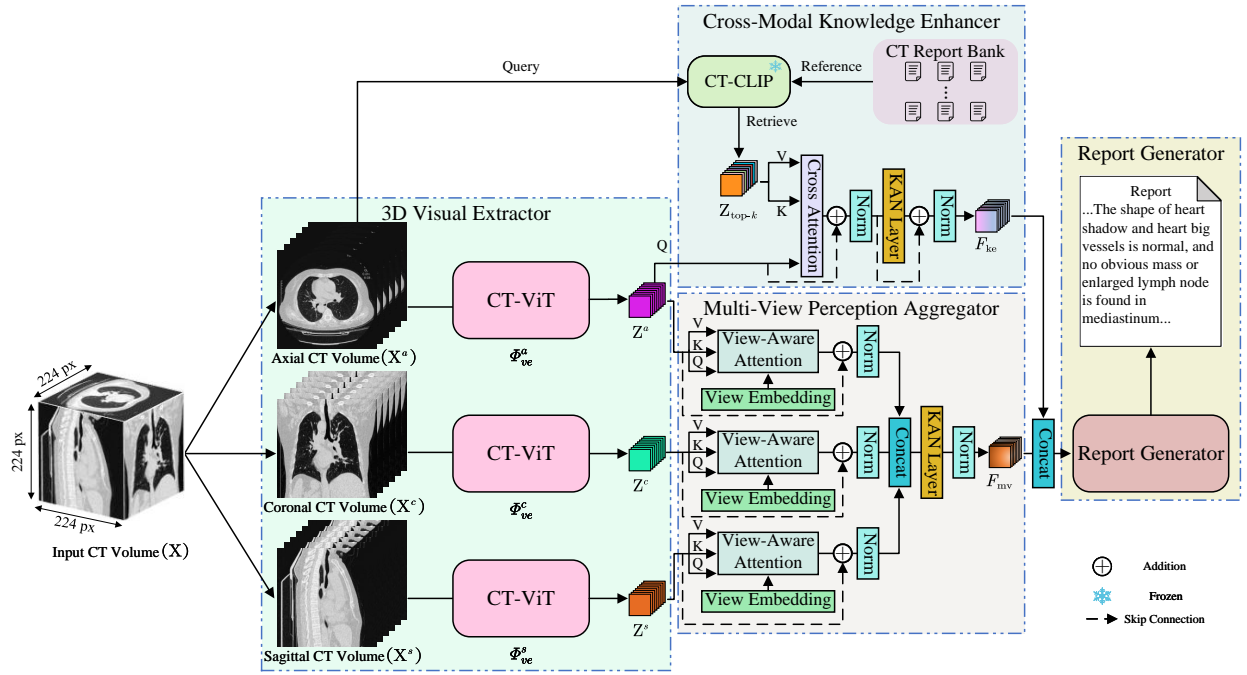


Fig. 2. The overview of our proposed MvKeTR, which can be partitioned into four parts: 3D visual extractor, multi-view perception aggregator, cross-modal knowledge enhancer, and report generator. The 3D visual extractor extracts CT patches from the axial, coronal, and sagittal view of the input 3D CT volume. Multi-view perception aggregator is devised to aggregate diagnostic information from multiple anatomical views effectively. Cross-modal knowledge enhancer is proposed to incorporate relevant clinical expertise into the diagnosis workflow. Report generator predicted the final reports relying on the multi-view diagnostic information and the related professional knowledge

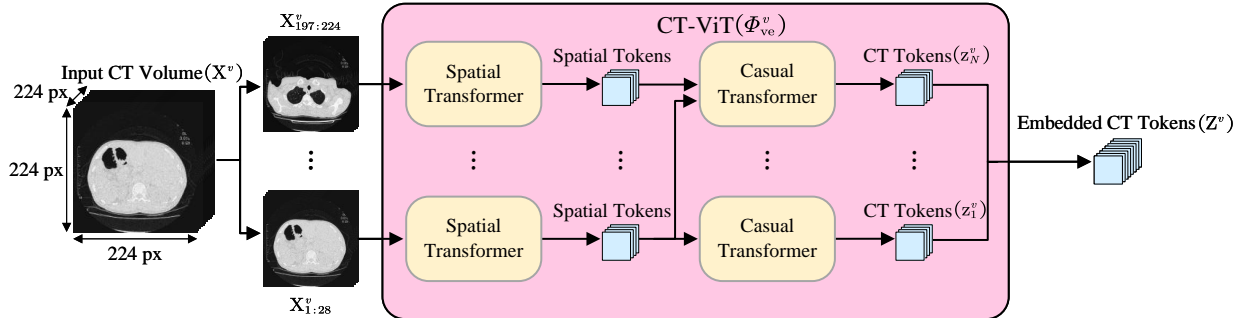


Fig. 3. Illustration of vision feature extraction pipeline through CT-ViT.

The learnable activation functions ϕ of the k^{th} KAN layer can be formalized as

$$\Phi_k = \{\phi_{i,j}\}, \quad i = 1, 2, \dots, N_{in}, \quad j = 1, 2, \dots, N_{out} \quad (7)$$

where $\phi_{i,j}$ represents functions with trainable parameters, and N_{in} and N_{out} denote the input and output dimensions, respectively. Then, the calculation of the KAN network from the k^{th} layer to the $(k+1)^{th}$ layer can be represented as:

$$\mathbf{x}_{k+1} = \Phi_k \mathbf{x}_k \quad (8)$$

Here, Φ_k is defined as a matrix form:

$$\Phi_k = \begin{pmatrix} \phi_{k,1,1}(\cdot) & \phi_{k,1,2}(\cdot) & \cdots & \phi_{k,1,n_k}(\cdot) \\ \phi_{k,2,1}(\cdot) & \phi_{k,2,2}(\cdot) & \cdots & \phi_{k,2,n_k}(\cdot) \\ \vdots & \vdots & \ddots & \vdots \\ \phi_{k,n_{k+1},1}(\cdot) & \phi_{k,n_{k+1},2}(\cdot) & \cdots & \phi_{k,n_{k+1},n_k}(\cdot) \end{pmatrix} \quad (9)$$

Inspired by KANs' promising potential, we explore using KANs as an alternative to traditional MLPs in the design of a

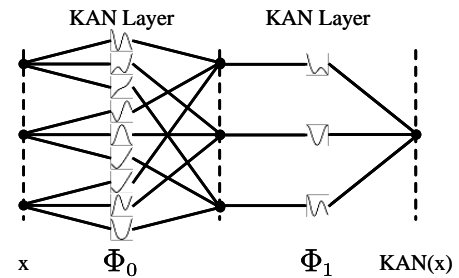


Fig. 4. The architecture of Kolmogorov-Arnold Networks (KANs) with a series of KAN layers.

multi-view perception aggregator and cross-modal knowledge enhancer.

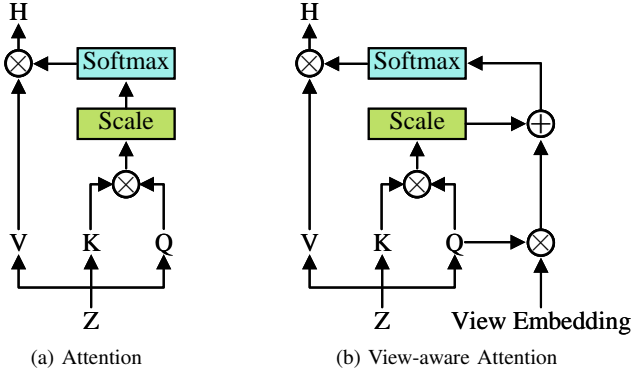


Fig. 5. The schematic diagram of Attention and View-aware Attention. “ \otimes ” denotes matrix multiplication. “ \oplus ” represents element-wise addition.

D. Multi-View Perception Aggregator

The multi-view perception aggregator is devised to perceive and aggregate diagnostic information from three orthogonal planes of the input CT volume: axial, coronal, and sagittal views. The details are presented below.

1) *View-aware Attention*: The vanilla attention (see Fig. 5a) adopted in Transformer [21] is computed through the correlation between the query matrix Q and the key matrix K , which is then used to aggregate information from the value matrix V . The process can be formulated as follows:

$$\text{Attention}(Q, K, V) = \text{Softmax}\left(\frac{QK^T}{\sqrt{d_k}}\right)V \quad (10)$$

where $Q = ZW_q$, $K = ZW_k$, $V = ZW_v$ are projected from the same input Z , $W_q \in \mathbb{R}^{D \times d_k}$, $W_k \in \mathbb{R}^{D \times d_k}$, $W_v \in \mathbb{R}^{D \times d_v}$ are learnable weight matrices.

This mechanism has proven effective in various tasks, particularly in capturing global dependencies. However, it fails to perceive the inherent distinctiveness between different views of the input CT volume, which can lead to suboptimal performance.

To effectively model the view-specific patterns, we design a view-aware attention module (see Fig. 5b), which introduces view embeddings E_v to characterize the uniqueness of each anatomical view explicitly. To be specific, given the query Q , key K , value V matrices, as well as E_v , view-aware attention is formulated as:

$$\begin{aligned} \text{VAA}_v &= \text{ViewAwareAttention}(Q, K, V, E_v) \\ &= \text{Softmax}\left(\frac{QK^T}{\sqrt{d_k}} + QE_v^T\right)V \end{aligned} \quad (11)$$

where $E_v \in \mathbb{R}^{N \times d_k}$, $v \in \{a, s, c\}$.

2) *Multi-view Aggregation*: After obtaining view-specific representations through Eq. (11), we propose a multi-view aggregation strategy to effectively combine the complementary information from multiple anatomical views while preserving their distinctive characteristics. First, for each view v , we normalize the attended values with residual connections:

$$\text{AN}_v = \text{Norm}(\text{VAA}_v + Z^v) \quad (12)$$

where Z^v denotes the embedded CT tokens from view v .

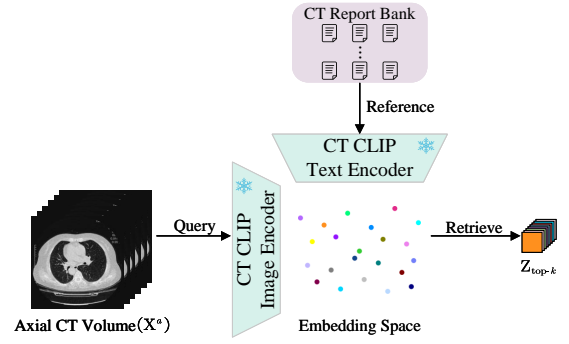


Fig. 6. Illustration of retrieving top- k report embeddings given a query CT volume.

To aggregate information across different views, we concatenate the normalized outputs from the axial, sagittal, and coronal views. This concatenated representation is then fused by a KAN layer, followed by a final normalization:

$$\begin{aligned} \text{Concat}_{mv} &= [\text{AN}_a; \text{AN}_s; \text{AN}_c] \\ F_{mv} &= \text{Norm}(\text{KANLayer}(\text{Concat}_{mv})) \end{aligned} \quad (13)$$

Here, $[\cdot; \cdot; \cdot]$ denotes the concatenation operation. We utilize the KAN layer instead of the traditional MLP layer to capture complex interactions between different views.

E. Cross-Modal Knowledge Enhancer

Analogous to clinicians’ diagnostic practice of consulting relevant medical records, the cross-modal knowledge enhancer is developed to integrate medical expertise into report generation. The entire procedure can be elaborated upon below.

1) *Volume-to-Report Retrieval*: As depicted in Fig. 6, we harness a well-trained CT-CLIP model on the CT-RATE dataset [40] to perform volume-to-report retrieval, which consists of an image encoder for CT volumes and a text encoder for reports. Given an input axial CT volume X^a and a CT report bank $R = \{R_1, R_2, \dots, R_{N_r}\}$ where R_i represents the i -th radiology report, N_r is the number of reports, we aim to retrieve the top- k most relevant report embeddings $Z_{\text{top-}k}$ from R . Here, to maintain consistency with CT-CLIP’s self-supervised pre-training, we utilize axial CT volume as query images for report retrieval.

The CT-CLIP image encoder E_{image} maps the input volume X^a to a D -dimensional embedding $v \in \mathbb{R}^D$:

$$v = E_{\text{image}}(X^a) \quad (14)$$

Similarly, each report R_i is encoded into a report embedding $r_i \in \mathbb{R}^D$ by the CT-CLIP text encoder E_{text} :

$$r_i = E_{\text{text}}(R_i) \quad (15)$$

After encoding both the input CT volume and reports into the shared embedding space, we apply L2 normalization to standardize the embeddings and compute the cosine similarity between them to retrieve the most relevant report embeddings:

$$\text{sim}(v, r_i) = \frac{v^T r_i}{\|v\| \|r_i\|} \quad (16)$$

$$Z_{\text{top-}k} = \arg \max_{r_i \in R'}^{\text{top-}k} \text{sim}(v, r_i) \quad (17)$$

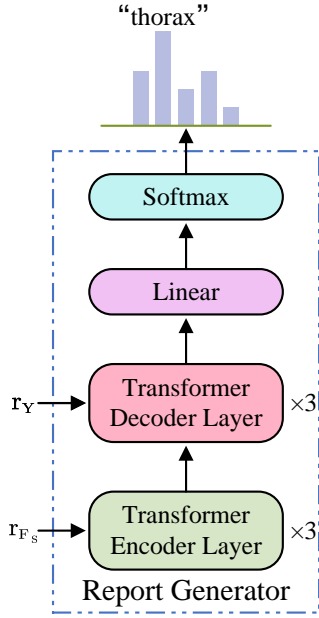


Fig. 7. Illustration of encoder-decoder architecture in report generator.

where $R' = \{r_1, r_2, \dots, r_{N_r}\}$ is the set of report embeddings.

2) Knowledge Enhancement: To effectively integrate visual features with retrieved medical knowledge, we introduce a knowledge enhancement mechanism. This mechanism employs a cross-attention module that enables the model to adaptively focus on relevant information from both the axial embedded CT tokens Z^a and the retrieved report embeddings $Z_{\text{top-k}}$. Specifically, given the query Q , key K , value V matrices, the cross-attention can be computed as follows:

$$\begin{aligned} \text{CA}_a &= \text{CrossAttention}(Q, K, V) \\ &= \text{Softmax}\left(\frac{QK^T}{\sqrt{d_k}}\right)V \end{aligned} \quad (18)$$

where $Q = Z^a W_q$, $K = Z_{\text{top-k}} W_k$, $V = Z_{\text{top-k}} W_v$, W_q , W_k , and W_v are learnable projection matrices. The output is further processed through residual connection and layer normalization:

$$\text{AN}_a = \text{Norm}(\text{CA}_a + Z^a) \quad (19)$$

Then, we process the enhanced features through a KAN layer followed by another residual connection and layer normalization:

$$F_{\text{ke}} = \text{Norm}(\text{KANLayer}(\text{AN}_a) + \text{AN}_a) \quad (20)$$

F. Report Generator

To efficiently produce reports, a significant body of recent works [5], [8]–[10], [32]–[36] adopt the encoder-decoder architecture, which is built upon standard transformer. We follow the R2GenCMN proposed by Chen et al. [5], which enhances the alignment between visual and textual modalities by introducing cross-modal memory networks (CMN). In detail, this network employs a learnable memory matrix and revise memory vectors by the attention mechanism during the multi-threaded querying and responding procedure, so as

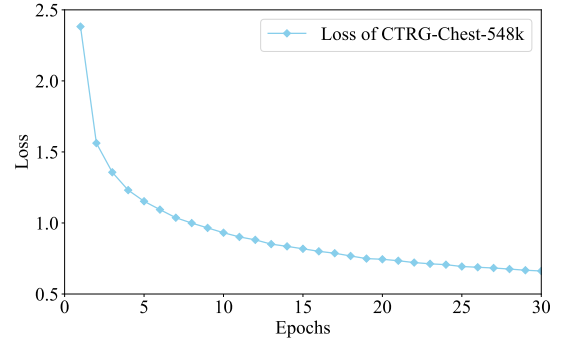


Fig. 8. The loss curve during training on the CTRG-Chest-548K.

to better align the visual and textual representations. Given a source sequence $F_S = \{f_1, f_2, f_3, \dots, f_S\}$ (concatenated features from the MVPA and CMKE modules for an input 3D CT volume), a target sequence $Y = \{y_1, y_2, y_3, \dots, y_T\}$, and a memory matrix $M = \{m_1, m_2, m_3, \dots, m_l\}$, the memory responses of F_S and Y can be obtained by:

$$r_{F_S} = \frac{F_S \cdot m_l^T}{\sqrt{d}} \cdot m_l \quad (21)$$

$$r_{y_t} = \frac{Y_T \cdot m_l^T}{\sqrt{d}} \cdot m_l \quad (22)$$

where l denotes the number of memory vectors, $m_j \in \mathbb{R}^d$ the memory vector at row j with d indicating its dimension. As illustrated in Fig. 7, the report generator of our model integrates a three-layer transformer with the above-mentioned cross-modal memory mechanism. The features encoded by MVPA and CMKE modules are concatenated and fed into this module, where the encoder processes only multi-modal features while the decoder takes only textual features as input. This process can be formulated as:

$$Z_S = R_e(r_{f_1}, r_{f_2}, \dots, r_{f_S}) \quad (23)$$

$$y_t = R_d(Z_S, r_{y_1}, r_{y_2}, \dots, r_{y_{(t-1)}}) \quad (24)$$

where $R_d(\cdot)$ and $R_e(\cdot)$ denote the decoder and encoder of the report generator, respectively, $\{r_{f_1}, r_{f_2}, \dots, r_{f_S}\}$ and $\{r_{y_1}, r_{y_2}, \dots, r_{y_{(t-1)}}\}$ represent the memory responses for multi-modal features and textual features from previously generated tokens, respectively, Z_S denotes the intermediate encoded states, y_t the predicted output at the current time step t . The complete report is produced by:

$$Y_t = \text{Softmax}(\text{Linear}(y_t)) \quad (25)$$

where $\text{Linear}(\cdot)$ and $\text{Softmax}(\cdot)$ denote the Linear and Softmax layer of the module, respectively, and Y_t represents the predicted token at time step t .

IV. EXPERIMENTS

A. Dataset

To validate the superiority of our proposed model, extensive experiments are carried out on the public chest CT report dataset CTRG-Chest-548K [8]¹, which encompasses 1,804

¹<https://github.com/tangyuhao2016/CTRG>

image-report pairs. Conforming to the same split proportion [8], 80% of the dataset is randomly allocated for training and 20% for testing.

As evident in Fig. 8, we present the loss value of the model trained on the CTRG-Chest-548K dataset. We can observe that the loss curve exhibits a consistent downward trend and eventually converges to a stable state.

B. Evaluation Metrics

The quality of the predicted reports is assessed through the most widely used evaluation metrics²: BLEU (i.e., BLEU-1, BLEU-2, BLEU-3, and BLEU-4) [41], METEOR [42], and ROUGE-L [43]. BLEU (Bilingual Evaluation Understudy) computes the overlap of n-grams between the candidate and reference reports and incorporates a brevity penalty to discourage overly short candidate sentences. METEOR (Metric for Evaluation of Translation with Explicit ORdering) extends beyond standard exact word matching by incorporating stemming and synonymy matching, which builds on the harmonic mean of unigram precision and recall, with more emphasis on recall than precision. ROUGE-L (Recall-Oriented Understudy for Gisting Evaluation-Longest Common Subsequence) calculates the longest common subsequence between the candidate and reference reports, allowing non-consecutive matches while maintaining word order.

C. Implementation Details

For both the compared methods and our method, CT-ViT [44] is employed as the 3D visual extractor, while all other configurations for the compared methods remain consistent with the original paper. The resolution of each CT volume is resized to $224 \times 224 \times 224$. The temporal and spatial patch sizes are both 28. The order of dimensions is transposed to form multi-view input volumes: axial view ($d \times h \times w$), sagittal view ($h \times d \times w$), and coronal view ($h \times w \times d$). Here, d stands for depth, h for height, and w for width. The top- k of CMKE is 16. The learning rates of the 3D visual extractor in the axial, coronal, and sagittal views, along with the other parameters, are set to 5×10^{-5} , 5×10^{-5} , 5×10^{-5} , and 1×10^{-4} , respectively. We decay the learning rate by a factor of 0.8 per epoch and set the beam size to 3. The model is trained with a batch size of 2 for 30 epochs using one NVIDIA RTX 4090 D, with Adam [45] as the optimizer and automatic mixed precision in PyTorch. The maximum length of generated reports is specified as 150. The words with a frequency of greater than 3 are retained, resulting in a vocabulary of 931 words.

D. Quantitative Analysis

To showcase the validity of the proposed MvKeTR, we compare it with the recent state-of-the-art methods, including CNN-RNN(i.e., MRMA [31]), CNN-Transformer(i.e., Vanilla Transformer [21], M2TR [32], R2GenCMN [5], TSGET [34],

UDT [35], CAMANet [36], CT2Rep [9], SL-DG [8]), knowledge base(i.e., M2KT [33]) and large language model(i.e., DiaLLaMA [10]). As Table II shows, on the CTRG-Chest-548K dataset, MvKeTR outperforms the recent SOTA approaches in all evaluation metrics by a considerable margin. Compared to MRMA, our method achieves an average gain of 17.13 across all metrics, with the most considerable improvement of 20.8 in ROUGE-L. Among CNN-Transformer methods, the vanilla Transformer yields relatively poor performance, showing a significant gap compared with our MvKeTR. More recent works like M2TR and R2GenCMN show improved performance but still fall behind our method. The latest transformer-based approaches, including TSGET, UDT, and CT2Rep, achieve competitive performance by proposing specialized architectural designs, while our method surpasses them all. M2KT achieves moderate performance, suggesting that merely incorporating knowledge base and additional disease labels may be insufficient. By adapting the pretrained LLaMA2-7B for CT report generation, DiaLLaMA shows promising results. However, there remains potential for further improvement. Notably, compared to the second-best method, CAMANet, our approach achieves an average improvement of 2.51 in terms of all metrics, demonstrating the superiority of our multi-view knowledge-enhanced architecture.

E. Qualitative Analysis

In addition to quantitative analysis, we also conduct qualitative analysis on test cases by comparing their ground truths with the reports generated from our proposed method, MvKeTR, and its baseline, R2GenCMN, upon which our method is built. Fig. 9 shows two examples from CTRG-Chest-548K and their corresponding reports where green and red highlights denote correct and incorrect content, respectively. In both cases, MvKeTR generates reports that resemble radiologists' observations in terms of clinical accuracy and professional terminology. To better illustrate the performance difference between MvKeTR and R2GenCMN, a detailed analysis of these two cases is presented below.

In the first case(top row of Fig.9), MvKeTR accurately detects key abnormalities such as increased lung transparency and patchy shadows in the left lower lobe. Although both methods make some errors in describing pleural effusion/thickening, MvKeTR provides a more comprehensive and accurate description similar to the ground truth report. For the second case (bottom row of Fig.9), MvKeTR successfully spots the presence of multiple nodules in both lungs, which is a critical diagnostic finding that R2GenCMN completely overlooks. These two cases suggest that MvKeTR not only provides more accurate and comprehensive reports but also shows better capability in detecting clinically significant abnormalities, which is essential for reliable medical diagnosis.

F. Ablation Study

Furthermore, we perform a body of ablation experiments to investigate the contributions of each component. The following baselines are used:

²<https://github.com/tylin/coco-caption>

TABLE II

THE PERFORMANCE COMPARISON OF OUR PROPOSED METHOD WITH RECENT SOTA WORKS ON THE TEST SET OF CTRG-CHEST-548K. ‡ DENOTES RESULTS DIRECTLY CITED FROM THE ORIGINAL PAPER. * REPRESENTS REPLICATED RESULTS BY THEIR PUBLIC CODES. THE BEST AND SECOND-BEST RESULTS ARE HIGHLIGHTED IN **BOLD** AND UNDERSCORED, RESPECTIVELY.

Method	Year	BLEU-1	BLEU-2	BLEU-3	BLEU-4	METEOR	ROUGE-L
Vanilla Transformer [21]*	2017	32.37	28.4	25.82	23.93	22.22	51.28
MRMA [31]*	2018	40.85	30.16	23.77	19.54	19.52	33.45
M2TR [32]*	2021	39.46	32.76	28.56	25.72	22.35	47.63
R2GenCMN [5]*	2022	48.29	38.34	32.53	28.42	23.89	48.91
M2KT [33]*	2023	39.71	33.17	29.12	26.16	20.11	47.19
TSGET [34]*	2024	46.12	38.15	32.92	28.84	23.02	50.19
UDT [35]*	2024	46.54	39.17	34.48	31.08	23.42	53.36
CAMANet [36]*	2024	<u>54.28</u>	<u>45.26</u>	<u>39.42</u>	<u>35.38</u>	<u>26.48</u>	<u>54.2</u>
CT2Rep [9]*	2024	49.81	40.7	35.19	31.28	24.82	51.18
SL-DG [8]‡	2024	-	-	-	23.70	21.90	43.80
Dia-LLaMA [10]‡	2024	51.16	-	-	29.64	26.28	42.15
MvKeTR(Ours)	-	58.36	48.79	42.43	37.86	28.36	54.25

All evaluation metrics are illustrated as percentage (%).

TABLE III

RESULTS OF ABLATION EXPERIMENTS. THE AVERAGE PERFORMANCE IMPROVEMENT OVER ALL METRICS COMPARED TO BASE IS PRESENTED IN THE "AVG. Δ" COLUMN. THE BEST RESULTS ARE HIGHLIGHTED IN **BOLD**.

Method	BLEU-1	BLEU-2	BLEU-3	BLEU-4	METEOR	ROUGE-L	AVG. Δ
BASE	48.29	38.34	32.53	28.42	23.89	48.91	-
BASE+MVPA	54.81	45.82	39.85	35.49	26.54	54.68	17.2%
BASE+CMKE	53.76	44.61	38.63	34.43	26.77	52.59	14.5%
Ours-MLP	53.98	45.3	39.55	35.39	27.16	54.05	14.1%
Ours	58.36	48.79	42.43	37.86	28.36	54.25	23.6%

All evaluation metrics are illustrated as percentage (%).



Input CT Volume	Ground Truth	R2GenCMN	Ours
	thorax is symmetrical trachea is in the middle . the markings of both lungs are slightly disordered the transparency of both lungs is increased and multiple small fine light transmission areas can be seen . the left lower lobe and the right lung showed multiple flocculent patchy and slightly high-density fuzzy shadows especially in the right lung the bronchial tube wall of the right lung was thickened . bilateral pulmonary hili are not large . the heart is enlarged and no mass or enlarged lymph node is found in the mediastinum . right pleural effusion right pleural thickening .	thorax is symmetrical no abnormality is found in rib and chest wall soft tissue . the lung window shows that the markings of both lungs are clear and natural the transparency of the lung field is good no abnormal consolidation is found in both lungs and the bilateral hilum is not large . the shape of heart shadow and large vessels is normal and no mass or enlarged lymph node is found in mediastinum . no pleural effusion or pleural hypertrophy .	thorax is symmetrical . the lung window shows that the bilateral lung markings are clear and natural . the transparency of the lung field is increased . patchy fuzzy shadows are seen in the lower lobe of the left lung and the bilateral pulmonary hili are not large . the shape of heart shadow and heart big vessels is normal and no obvious mass or enlarged lymph node is found in mediastinum . no pleural effusion or pleural thickening .
	thorax is symmetrical bilateral lung markings are clear the walking is natural the lung field transmittance is good multiple small nodules are seen in both lungs the diameter is not more than 5mm and bilateral pulmonary hili are not large . the shape of heart shadow and large vessels is normal and no mass or enlarged lymph node is found in mediastinum . no pleural effusion or pleural hypertrophy .	thorax is symmetrical no abnormality is found in rib and chest wall soft tissue . the lung window shows that the markings of both lungs are clear and natural the transparency of the lung field is good no abnormal consolidation is found in both lungs and the bilateral hilum is not large . the shape of heart shadow and large vessels is normal and no mass or enlarged lymph node is found in mediastinum . no pleural effusion or pleural hypertrophy .	thorax is symmetrical . the lung window shows that the bilateral lung markings are clear and natural . the lung field transparency is good . multiple ground glass nodules are seen in both lungs . the larger one is located in the upper lobe of the right lung with a diameter of about 0 . 5cm and the bilateral pulmonary hili are not large . the shape of heart shadow and heart big vessels is normal and no obvious mass or enlarged lymph node is found in mediastinum . no pleural effusion or pleural thickening .

Fig. 9. The examples of report from ground-truth, R2GenCMN, and our method. Green/red highlights denotes correct/incorrect content respectively.

- BASE: The base model employs CT-ViT as the 3D visual extractor and the encoder-decoder of R2GenCMN as the report generator.
 - BASE+MVPA: The base model enhanced with the proposed multi-view perception aggregator.
 - BASE+CMKE: The base model integrated with the proposed cross-modal knowledge enhancer.
 - Ours-MLP: This is the complete model with KAN layers replaced by MLP layers.
 - Ours: This is the complete model with all proposed components.
- As shown in Table III, we can draw several key obser-

TABLE IV
THE PERFORMANCE COMPARISON OF THE MVKETR FRAMEWORK UNDER DIFFERENT 3D VISUAL EXTRACTOR. THE BEST RESULTS ARE HIGHLIGHTED IN **BOLD**.

Visual Extractor	BLEU-1	BLEU-2	BLEU-3	BLEU-4	METEOR	ROUGE-L
3D ViT [46]	58.39	47.27	39.87	34.59	26.99	49.43
CT-Net [47]	50.1	42.24	37.03	33.33	26.17	53.67
U-Net [48]	48.55	39.87	34.72	31.1	24.75	52.27
CT-ViT [44]	58.36	48.79	42.43	37.86	28.36	54.25

All evaluation metrics are illustrated as percentage (%).

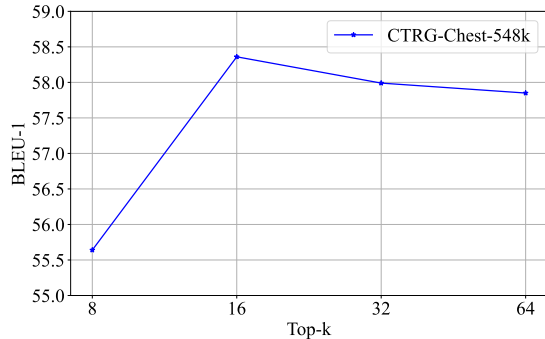


Fig. 10. Effect of varying top-k on CTRG-Chest-548K.

variations. First, compared to BASE, BASE+MVPA achieves an average improvement of 17.2%, which confirms the efficacy of integrating diagnostic information across multiple anatomical views through view-aware attention. Second, BASE+CMKE shows a 14.5% average improvement over BASE, indicating the usefulness of incorporating medical expertise from similar cases. Particularly, BASE+MVPA achieves better performance than BASE+CMKE. This observation is attributed to the fact that multi-view perception is more crucial than clinical knowledge enhancement. Third, the comparison between Ours-MLP and Ours reveals a performance gap of 9.5% (23.6% vs 14.1% in average improvement). This observation owes to the fact that KAN layers are more effective in modeling complicated diagnostic relationships compared to conventional MLP layers.

When combining all components, Ours achieves the best overall performance with a 23.6% average improvement over BASE. This suggests that multi-view perception, knowledge enhancement, and KAN network work complementarily in improving the quality of CT reports.

G. Discussion

1) *Comparison of different 3D visual extractors*: We conduct experiments to assess the impact of various 3D visual extractors, including CNN-based methods: U-Net [48], and CT-Net [47] as well as recent ViT-based methods: 3D ViT [46], and CT-ViT [44]. As demonstrated in Table IV, we find that CT-ViT (see Fig. 3) is the most suitable 3D visual extractor for our proposed MvKeTR, which leverages the advantages of two types of transformers: spatial transformers and causal transformers. Specifically, the spatial transformers excel at capturing local spatial features and relationships within CT slices, which is crucial for understanding anatomical structures and lesion locations. Meanwhile, the causal transformers are

adept at modeling long-range dependencies across different slices or depth levels of the 3D CT volume, ensuring comprehensive feature extraction. This combination effectively preserves spatial and volumetric information throughout the 3D visual feature extraction pipeline. Moreover, the ViT-based methods show relatively higher performance compared to the CNN-based counterparts, suggesting that the self-attention mechanism is more effective in capturing global dependencies and long-range interactions within visual features, which is crucial for CT report generation.

2) *Effect of varying top-k*: The top- k is a key hyperparameter of CMKE module, which determines the number of most relevant reports to be retrieved for the current report generation. As revealed in Fig. 10, we observe that increasing the top- k at first improves the BLEU-1 score, reaching a peak at top- $k=16$, beyond which the performance deteriorates. This trend suggests that while retrieving more relevant reports provides richer reference information, excessive retrieval beyond a certain threshold may introduce noise without additional benefits. Hence, the top- k is set to 16, balancing performance gains and computational efficiency.

V. CONCLUSION

In this paper, we present MvKeTR, a novel framework that integrates multi-view perception and knowledge enhancement for high-quality radiology report generation from 3D CT volumes. First, multi-view features are extracted by a 3D visual extractor, which comprises three separate CT-ViT networks. The multi-view perception aggregator is then utilized to synthesize visual features from three anatomical views. Following this, the cross-modal knowledge enhancer is responsible for incorporating clinical knowledge from the most relevant cases into the diagnostic process. Finally, these features encoded by the two aforementioned modules are concatenated and fed into the report generator to produce the final report. Experimental results on the CTRG-Chest-548K dataset demonstrate the superiority of our method over prior state-of-the-art studies.

Notwithstanding our contributions in automatic radiology report generation, there are still limitations. In future work, we will focus on validating the generalizability and effectiveness of our proposed model through a real-world pilot study across local hospitals and extending the framework to other 3D medical imaging modalities (e.g., MRI) and different body parts.

REFERENCES

- [1] S. K. Goergen, F. J. Pool, T. J. Turner, J. E. Grimm, M. N. Appleyard, C. Crock, M. C. Fahey, M. F. Fay, N. J. Ferris, S. M. Liew *et al.*,

- “Evidence-based guideline for the written radiology report: Methods, recommendations and implementation challenges,” *J. Med. Imaging Radiat. Oncol.*, vol. 57, no. 1, pp. 1–7, 2013.
- [2] A. B. Rosenkrantz, D. R. Hughes, and R. Duszak Jr, “The us radiologist workforce: an analysis of temporal and geographic variation by using large national datasets,” *Radiology*, vol. 279, no. 1, pp. 175–184, 2016.
 - [3] A. Rimmer, “Radiologist shortage leaves patient care at risk, warns royal college,” *BMJ-BRIT. MED. J.*, vol. 359, 2017.
 - [4] M. A. Bruno, E. A. Walker, and H. H. Abujudeh, “Understanding and confronting our mistakes: the epidemiology of error in radiology and strategies for error reduction,” *Radiographics*, vol. 35, no. 6, pp. 1668–1676, 2015.
 - [5] Z. Chen, Y. Shen, Y. Song, and X. Wan, “Cross-modal memory networks for radiology report generation,” in *Proc. 59th Ann. Meeting Assoc. Comput. Linguistics, 11th Int. Joint Conf. Natural Lang. Process*, 2021, pp. 5904–5914.
 - [6] Y. Jin, W. Chen, Y. Tian, Y. Song, C. Yan, and Z. Mao, “Improving radiology report generation with d 2-net: When diffusion meets discriminator,” in *Proc. IEEE Int. Conf. Acoust. Speech Signal Process.*, 2024, pp. 2215–2219.
 - [7] N. Müller, “Computed tomography and magnetic resonance imaging: past, present and future,” *Eur. Respir. J.*, vol. 19, no. 35 suppl, pp. 3s–12s, 2002.
 - [8] Y. Tang, H. Yang, L. Zhang, and Y. Yuan, “Work like a doctor: Unifying scan localizer and dynamic generator for automated computed tomography report generation,” *Expert Syst. Appl.*, vol. 237, p. 121442, 2024.
 - [9] I. E. Hamamci, S. Er, and B. Menze, “Ct2rep: Automated radiology report generation for 3d medical imaging,” *arXiv:2403.06801*, 2024.
 - [10] Z. Chen, L. Luo, Y. Bie, and H. Chen, “Dia-llama: Towards large language model-driven ct report generation,” *arXiv:2403.16386*, 2024.
 - [11] A. A. A. Setio, F. Ciompi, G. Litjens, P. Gerke, C. Jacobs, S. J. Van Riel, M. M. W. Wille, M. Naqibullah, C. I. Sánchez, and B. Van Ginneken, “Pulmonary nodule detection in ct images: false positive reduction using multi-view convolutional networks,” *IEEE Trans. Med. Imaging*, vol. 35, no. 5, pp. 1160–1169, 2016.
 - [12] A. A. Bankier, H. MacMahon, J. M. Goo, G. D. Rubin, C. M. Schaefer-Prokop, and D. P. Naidich, “Recommendations for measuring pulmonary nodules at ct: a statement from the fleischner society,” *Radiology*, vol. 285, no. 2, pp. 584–600, 2017.
 - [13] H. MacMahon, D. P. Naidich, J. M. Goo, K. S. Lee, A. N. Leung, J. R. Mayo, A. C. Mehta, Y. Ohno, C. A. Powell, M. Prokop *et al.*, “Guidelines for management of incidental pulmonary nodules detected on ct images: from the fleischner society 2017,” *Radiology*, vol. 284, no. 1, pp. 228–243, 2017.
 - [14] Z. Chen, Y. Song, T.-H. Chang, and X. Wan, “Generating radiology reports via memory-driven transformer,” in *Proc. Conf. Empirical Methods Natural Lang. Process.*, Nov. 2020, pp. 1439–1449.
 - [15] Z. Liu, Y. Wang, S. Vaidya, F. Ruehle, J. Halverson, M. Soljačić, T. Y. Hou, and M. Tegmark, “Kan: Kolmogorov-arnold networks,” *arXiv:2404.19756*, 2024.
 - [16] S. Bai and S. An, “A survey on automatic image caption generation,” *Neurocomputing*, vol. 311, pp. 291–304, 2018.
 - [17] H. Wang, Y. Zhang, and X. Yu, “An overview of image caption generation methods,” *Comput. Intell. Neurosci.*, vol. 2020, no. 1, p. 3062706, 2020.
 - [18] O. Vinyals, A. Toshev, S. Bengio, and D. Erhan, “Show and tell: A neural image caption generator,” in *Proc. IEEE Conf. Comput. Vis. Pattern Recognit.*, 2015, pp. 3156–3164.
 - [19] S. J. Rennie, E. Marcheret, Y. Mroueh, J. Ross, and V. Goel, “Self-critical sequence training for image captioning,” in *Proc. IEEE Conf. Comput. Vis. Pattern Recognit.*, 2017, pp. 7008–7024.
 - [20] B. Z. Yao, X. Yang, L. Lin, M. W. Lee, and S.-C. Zhu, “I2t: Image parsing to text description,” *Proceedings of the IEEE*, vol. 98, no. 8, pp. 1485–1508, 2010.
 - [21] A. Vaswani, N. Shazeer, N. Parmar, J. Uszkoreit, L. Jones, A. N. Gomez, L. Kaiser, and I. Polosukhin, “Attention is all you need,” in *Proc. 31st Int. Conf. Neural Inf. Process. Syst.*, 2017, p. 6000–6010.
 - [22] K. Xu, “Show, attend and tell: Neural image caption generation with visual attention,” *arXiv:1502.03044*, 2015.
 - [23] L. Li, S. Tang, L. Deng, Y. Zhang, and Q. Tian, “Image caption with global-local attention,” in *Proc. AAAI Conf. Artif. Intell.*, vol. 31, no. 1, 2017.
 - [24] J. Lu, C. Xiong, D. Parikh, and R. Socher, “Knowing when to look: Adaptive attention via a visual sentinel for image captioning,” in *Proc. IEEE Conf. Comput. Vis. Pattern Recognit.*, 2017, pp. 375–383.
 - [25] M. Cornia, M. Stefanini, L. Baraldi, and R. Cucchiara, “Meshed-memory transformer for image captioning,” in *Proc. IEEE Conf. Comput. Vis. Pattern Recognit.*, 2020, pp. 10578–10587.
 - [26] W. Liu, S. Chen, L. Guo, X. Zhu, and J. Liu, “Cptr: Full transformer network for image captioning,” *arXiv:2101.10804*, 2021.
 - [27] B. Jing, P. Xie, and E. Xing, “On the automatic generation of medical imaging reports,” *arXiv:1711.08195*, 2017.
 - [28] Y. Xue, T. Xu, L. Rodney Long, Z. Xue, S. Antani, G. R. Thoma, and X. Huang, “Multimodal recurrent model with attention for automated radiology report generation,” in *Proc. Int. Conf. Med. Image Comput. Comput.-Assisted Intervention*, 2018, pp. 457–466.
 - [29] A. Hoogi, A. Mishra, F. Gimenez, J. Dong, and D. Rubin, “Natural language generation model for mammography reports simulation,” *IEEE J. Biomed. Health Inform.*, vol. 24, no. 9, pp. 2711–2717, 2020.
 - [30] Z. Wang, L. Zhou, L. Wang, and X. Li, “A self-boosting framework for automated radiographic report generation,” in *Proc. IEEE Conf. Comput. Vis. Pattern Recognit.*, 2021, pp. 2433–2442.
 - [31] Y. Xue, T. Xu, L. Rodney Long, Z. Xue, S. Antani, G. R. Thoma, and X. Huang, “Multimodal recurrent model with attention for automated radiology report generation,” in *Proc. 21st Int. Conf. Med. Image Comput. Comput.-Assisted Intervention*, 2018, pp. 457–466.
 - [32] F. Nooralahzadeh, N. Perez Gonzalez, T. Frauenfelder, K. Fujimoto, and M. Krauthammer, “Progressive transformer-based generation of radiology reports,” in *Proc. Findings Assoc. Comput. Linguistics: EMNLP 2021*, 2021, pp. 2824–2832.
 - [33] S. Yang, X. Wu, S. Ge, Z. Zheng, S. K. Zhou, and L. Xiao, “Radiology report generation with a learned knowledge base and multi-modal alignment,” *Med. Image Anal.*, vol. 86, p. 102798, 2023.
 - [34] X. Yi, Y. Fu, R. Liu, H. Zhang, and R. Hua, “Tsget: Two-stage global enhanced transformer for automatic radiology report generation,” *IEEE J. Biomed. Health Inform.*, vol. 28, no. 4, pp. 2152–2162, 2024.
 - [35] X. Yi, Y. Fu, R. Hua, R. Liu, and H. Zhang, “Unsupervised disease tags for automatic radiology report generation,” *Biomed Signal Process Control*, vol. 89, p. 105742, 2024.
 - [36] J. Wang, A. Bhalerao, T. Yin, S. See, and Y. He, “Camagnet: Class activation map guided attention network for radiology report generation,” *IEEE J. Biomed. Health Inform.*, vol. 28, no. 4, pp. 2199–2210, 2024.
 - [37] D. E. Rumelhart, G. E. Hinton, and R. J. Williams, “Learning representations by back-propagating errors,” *nature*, vol. 323, no. 6088, pp. 533–536, 1986.
 - [38] K. Hornik, M. Stinchcombe, and H. White, “Multilayer feedforward networks are universal approximators,” *Neural networks*, vol. 2, no. 5, pp. 359–366, 1989.
 - [39] C. Li, X. Liu, W. Li, C. Wang, H. Liu, and Y. Yuan, “U-kan makes strong backbone for medical image segmentation and generation,” *arXiv:2406.02918*, 2024.
 - [40] I. E. Hamamci, S. Er, F. Almas, A. G. Simsek, S. N. Esirgun, I. Dogan, M. F. Dasdelen, B. Wittmann, E. Simsar, M. Simsar *et al.*, “A foundation model utilizing chest ct volumes and radiology reports for supervised-level zero-shot detection of abnormalities,” *arXiv:2403.17834*, 2024.
 - [41] K. Papineni, S. Roukos, T. Ward, and W.-J. Zhu, “Bleu: a method for automatic evaluation of machine translation,” in *Proc. 40th Annu. Meeting Assoc. Comput. Linguistics*, Jul. 2002, pp. 311–318.
 - [42] M. Denkowski and A. Lavie, “Meteor 1.3: Automatic metric for reliable optimization and evaluation of machine translation systems,” in *Proc. 6th Workshop Stat. Mach. Transl.*, 2011, pp. 85–91.
 - [43] C.-Y. Lin, “ROUGE: A package for automatic evaluation of summaries,” in *Proc. Text Summarization Branches Out*, Jul. 2004, pp. 74–81.
 - [44] I. E. Hamamci, S. Er, A. Sekuboyina, E. Simsar, A. Tezcan, A. G. Simsek, S. N. Esirgun, F. Almas, I. Dogan, M. F. Dasdelen *et al.*, “Generatect: Text-conditional generation of 3d chest ct volumes,” *arXiv:2305.16037*, 2023.
 - [45] D. P. Kingma and J. Ba, “Adam: A method for stochastic optimization,” *arXiv:1412.6980*, 2014.
 - [46] A. Dosovitskiy, L. Beyer, A. Kolesnikov, D. Weissenborn, X. Zhai, T. Unterthiner, M. Dehghani, M. Minderer, G. Heigold, S. Gelly, J. Uszkoreit, and N. Houlsby, “An image is worth 16x16 words: Transformers for image recognition at scale,” in *Proc. Int. Conf. Learn. Represent.*, 2021.
 - [47] R. L. Draelos, D. Dov, M. A. Mazurowski, J. Y. Lo, R. Henao, G. D. Rubin, and L. Carin, “Machine-learning-based multiple abnormality prediction with large-scale chest computed tomography volumes,” *Med. Image Anal.*, vol. 67, p. 101857, 2021.
 - [48] O. Ronneberger, P. Fischer, and T. Brox, “U-net: Convolutional networks for biomedical image segmentation,” in *Proc. Int. Conf. Med. Image Comput. Comput.-Assisted Intervention*, 2015, pp. 234–241.